frontiers | Frontiers in Built Environment

TYPE Original Research
PUBLISHED 01 March 2024
DOI 10.3389/fbuil.2024.1333937

OPEN ACCESS

EDITED BY
Yong Tan,
Tongji University, China

REVIEWED BY
Liseane Padilha Thives,
Federal University of Santa Catarina, Brazil
Ayhan Gurbuz,
Gazi University, Türkiye

*CORRESPONDENCE
LeiKe Luo,
1419354603@qq.com

RECEIVED 06 November 2023
ACCEPTED 04 January 2024
PUBLISHED 01 March 2024

CITATION
Xie X, Yang G, Liu Z, Tang Y, Chu J, Wen W, Chen A, Guo J and Luo L (2024), Field experiment on a vegetation-wicking geotextile-reinforced base for a permeable sidewalk. *Front. Built Environ.* 10:1333937. doi: 10.3389/fbuil.2024.1333937

Field experiment on a vegetation-wicking geotextile-reinforced base for a permeable sidewalk

Xiangbin Xie[1], Gengxin Yang[1], Zhao Liu[1], Yelin Tang[1], Jingying Chu[2], Wenhao Wen[3], Aolong Chen[3], Jun Guo[3] and LeiKe Luo[3]*

[1]Chn Energy Dadu River Zhensha Hydropower Construction Management Branch, Leshan, China, [2]Tencate Industrial Zhuhai Co. Ltd., Zhuhai, China, [3]College of Civil and Transportation Engineering, Shenzhen University, Shenzhen, China

Wicking geotextiles have proven effective in reducing water content in road bases under both saturated and unsaturated conditions, thereby increasing granular base strength and mitigating moisture-related damage to the pavement. Despite their effectiveness in paved roads, the use of wicking geotextiles in permeable road and sidewalk, particularly in areas requiring robust drainage such as sponge cities, is not well explored. In "sponge city" roads, moisture content fluctuations and subsequent damage to the structure often cause concern, and the wicking geotextile's drainage could be a potential solution. Therefore, this study aims to investigate and quantify the effectiveness of wicking geotextiles in reducing the moisture content and improving the resilient modulus of permeable sidewalk base layers. The moisture contents of unstabilized and one-directional wicking geotextile- and two-directional wicking geotextile-stabilized bases under permeable paving bricks were monitored with an interval of 7–10 days for over a year. An analytical approach to reconstruct daily moisture content in the base layer was proposed based on the simulated rainfall saturation test. This approach further assesses the enhancements in resilient modulus due to the drainage capabilities of wicking geotextiles. The experimental results indicated that the two-directional wicking geotextile outperforms its one-directional counterpart and both wicking geotextiles outperformed the control condition in terms of drainage efficiency. By reconstructing the daily moisture content and utilizing the relative damage model, the two-directional wicking geotextile significantly improved the annual equivalent resilient modulus of the base layer under permeable paving bricks.

KEYWORDS

geosynthetics, geotextile, suction, wicking, base course, water content

1 Introduction

1.1 Designing concern of permeable road

With the rapid progression of urban construction, an increasing amount of natural ground surface is being replaced by impermeable paving materials such as asphalt, cement, and concrete (Moore et al., 2016; Zhang et al., 2018; Chen et al., 2019; Coseo and Larsen, 2019). While blocking the water transfer channel between rainfall and soil,

these materials have also caused surges in the surface runoff in the cities; thus, floods and waterlogging occur frequently in the cities (Radfar and Rockaway, 2016; Coble et al., 2018; Li et al., 2018; Qin et al., 2019). In order to reduce the flow of generated runoff, some scholars analyzed different low-impact development (LID) practices based on field experiments and found that LID practices have a greater impact on the ability to reduce surface runoff (Shafique and Kim, 2017; Shakya et al., 2019). Permeable sidewalk is an effective LID practice that plays an important role in reducing rainfall runoff in urban areas. The permeable sidewalk allows rainwater to penetrate the surface layer while reducing the pressure on the drainage system. Typically, in permeable pavements, water is allowed to penetrate the surface layer and be transported within the base layer. Thus, the base layer quality often plays an essential role in the durability of permeable pavements.

1.2 Moisture-related pavement issues

Base course deterioration due to excessive moisture represents a primary factor contributing to pavement distress, including surface deformation and cracking in both asphalt and concrete pavements [the Federal Highway Administration (FHWA), 1992; Reebie Associates, Economic Development Research Group, Carl Martland (2004)]. The 1993 American Association of State Highway and Transportation Officials (AASHTO) Guide for Design of Pavement Structures and the Mechanistic-Empirical Pavement Design Guide (MEPDG) incorporate base course moisture conditions into their designs. Hence, it is imperative to effectively manage moisture within the base course and maintain a relatively low moisture content to minimize pavement distress. Traditional drainage layers in roadway sections have historically utilized open-graded aggregates or, more recently, geosynthetics such as geotextiles or geo-composites for drainage. However, drainage materials relying solely on gravity to remove water may experience reduced efficiency as the base course and drainage materials become unsaturated (Iryo and Rowe, 2004; Garcia et al., 2007; McCartney and Zornberg, 2010). A series of rainfall simulation studies conducted on embankment models by Garcia et al. (2007) indicate that a non-woven geotextile behaves as a capillary barrier during infiltration, resulting in high saturation of the geological material above the geotextile. This behavior can be attributed to the hydrophobic and water-repellent nature of the synthetic materials used to construct traditional geotextiles, such as polyesters and polypropylenes, as highlighted by Koerner (2012). Consequently, similar to soil, the drainage efficiency of the geotextile decreases with the level of saturation. The drainage of the geotextile occurs primarily under saturated conditions, relying on gravity. However, roadway structures spend most of their time in unsaturated conditions, limiting the drainage capability of the conventional geotextile. While traditional drainage materials effectively remove water from saturated base courses, unsaturated base courses may retain excessive moisture, leading to pavement distress. In addition, in sidewalk construction, the base layer often employs cost-effective materials, avoiding well-graded crushed stone. Instead, materials with a higher proportion of fine particles are commonly used. Such materials are more susceptible to moisture content effects, highlighting the increased importance of drainage.

1.3 Wicking geotextile drainage stabilization mechanism

The advancement of geosynthetics has led to the emergence of a novel geotextile, known as the wicking geotextile, which is infused with water-absorbent fibers. Research has shown that wicking geotextiles generate suction, actively drawing moisture from the surrounding geomaterials and facilitating drainage in unsaturated conditions while maintaining the mechanical reinforcement properties of traditional geotextiles. The incorporation of wicking fibers substantially increases the water-absorption capacity and elevates the air entry value of these geotextiles (Lin and Zhang, 2020). As a result, wicking geotextiles not only enhance drainage in saturated aggregate bases but also effectively reduce moisture in unsaturated matrices. This process, known as capillary drainage, involves the removal of capillary water from unsaturated aggregates through the suction action of wicking geotextiles (Wang et al., 2017). The underlying principles of capillary drainage have been delineated in studies conducted by Han and Zhang (2014), Wang et al. (2017), and Guo et al. (2017). Column tests by Guo et al. (2019) and Bai and Liu (2021) have demonstrated that wicking geotextiles significantly lower the soil moisture content up to a certain depth above the geotextile layer. Additionally, Hachem and Zornberg (2019) conducted experimental evaluations of the dewatering capacity of wicking geotextiles, particularly in scenarios involving rising groundwater at the interface of the base and subgrade layers.

A plethora of studies have evaluated the efficacy of wicking geotextiles. For example, Wang et al. (2017) conducted a laboratory study in which a wicking geotextile was placed at the interface between the soil and base to examine its ability to reduce soil moisture following simulated rainfall. Their findings revealed that the wicking geotextile effectively reduced the water content in the base by employing both gravity and suction for drainage. Similarly, Lin and Zhang (2019) observed moisture content fluctuations in a large-scale sandbox, discovering that the wicking geotextile could remove water from sand utilizing the same mechanisms. Alvarenga et al. (2021) further affirmed the capability of the wicking geotextile to regulate base moisture content even during spring thaw, showcasing its effectiveness under unsaturated conditions. In their research, Lin et al. (2019) generated soil-water characteristic curves for both wicking and non-wicking geotextiles, demonstrating that wicking geotextile varieties offer superior water retention and drainage capacity. Moreover, Bai and Liu (2021) explored how various fiber parameters in wicking geotextiles affect their drainage efficiency through column tests, observing optimal performance in unidirectional absorbent fibers with 3 mm fiber spacing in unsaturated clay. Laprade and Lostumbo (2020) reviewed the applications of wicking geotextiles in road drainage over the last decade, concluding that these fabrics are highly effective in reducing water content in road subgrades under unsaturated conditions and enhancing subgrade resilience. Additionally, Guo et al. (2016) investigated the maximum dewatering rate of the

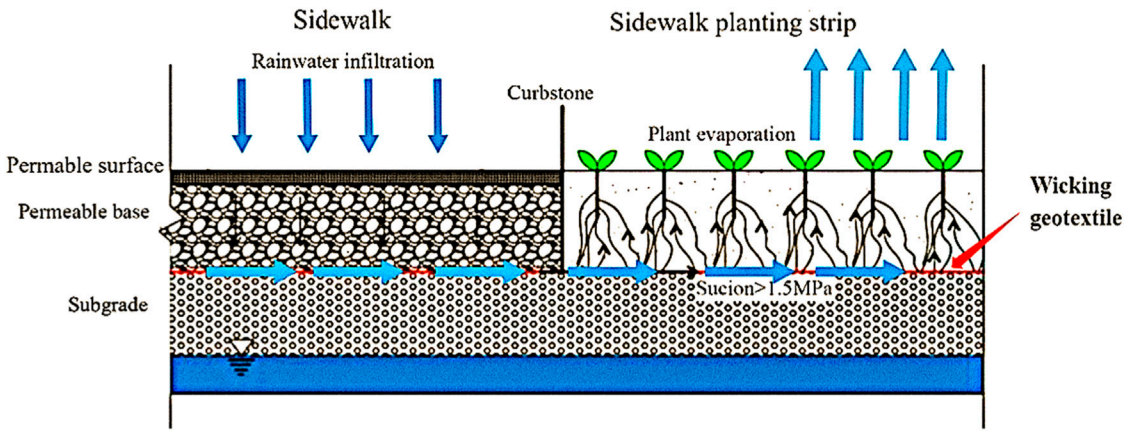

FIGURE 1
Schematic of the vegetation-wicking geotextile permeable sidewalk.

wicking geotextile under controlled conditions in a water tank, introducing the concept of equivalent evaporation length as a measure of the geotextile's dewatering capacity.

Garcia et al. (2007) conducted laboratory tests to explore the hydraulic behavior of geosynthetic materials in unsaturated road embankments during heavy rainfall. Their findings revealed that wicking geotextiles effectively reduce water accumulation during infiltration, thereby preventing deformation of the foundation. Consequently, wicking geotextiles are efficient in draining water from road subgrades and improving their resilience modulus. Guo et al. (2017) developed a design method grounded in the 1993 AASHTO relative damage model, considering the mechanical and drainage stabilization effects of wicking geotextiles. However, this method primarily addresses rainfall events leading to base saturation and overlooks moisture content variations in the base material due to less-intense or continuous rain. To address this gap, Lin et al. (2019) introduced a novel design method using a numerical model. This method encompasses a coupled mechanical model that simulates the interaction between soil, vegetation, and climate, employing finite element methods to mimic the elastic behavior of unsaturated pavement structures, both with and without a wicking geotextile, thereby calculating the equivalent resilience modulus for each pavement layer. This approach integrates the benefits of the wicking geotextile into both the 1993 AASHTO and the MEPDG specifications. However, it primarily enhances road structural performance under simulated climatic conditions and may not fully represent real-world scenarios. Moreover, the influence of plant suction on the road base requires further investigation.

1.4 Hydrodynamic integration of wicking geotextiles in permeable sidewalk systems

In this study, a permeable sidewalk design, as depicted in Figure 1, was introduced. Wicking geotextiles efficiently extract moisture from the soil, while plants simultaneously desiccate the underlying soil through transpiration. The transpiration suction, significantly exceeding the matric suction, readily draws water from the geotextile, thereby establishing a sustained humidity gradient. This gradient actively drives water from the geotextiles beneath the sidewalk toward those situated directly under the plant roots. The geotextile's soil-analogous pore structure significantly enhances water infiltration and retention, fostering robust root anchorage to the geotextile due to the roots' hygroscopic nature. Consequently, this arrangement offers a consistent moisture supply and robust structural support to the plants. This design allows rainwater infiltrating the sidewalk to be used for irrigating adjacent vegetation. The wicking geotextile, positioned between the subgrade and the base course, extends into the vegetation area. Following rainfall, the permeable pavement aids in directing rainwater into the sidewalk base, increasing the moisture content near the wicking geotextile. The vegetation in the sidewalk planting strip, requiring substantial water for metabolic processes and transpiration, generates high suction through the roots, extracting moisture from the surrounding soil. Consequently, the section of the wicking geotextile beneath the vegetation exhibits higher suction compared to that under the sidewalk. This difference in suction drives the moisture movement from the sidewalk toward the planting strip, effectively removing moisture from the road structure.

1.5 Exploring the application of wicking geotextiles from roads to sidewalks

The predominant focus of existing research on wicking geotextiles has been their application in road construction. The utilization of traditional geotextiles in sidewalks is generally analogous to their use in roads, considering that the construction methods for sidewalks and roads share fundamental similarities, including subgrade, subbase, base, and surface layers. However, sidewalk design standards for load bearing are typically lower than those for roads, often involving materials of lower strength, which frequently contain much finer particles. To ensure effective drainage without impairing the functionality of main roads during heavy rainfall, rainwater is often channeled to the sides, accumulating in the sidewalk base. Consequently, sidewalks endure not only the direct impact of descending rainwater but also a portion of the drainage load from the roads, subjecting them

to greater water content fluctuations than the roads. This suggests that employing wicking geotextiles in sidewalks could yield additional benefits in enhancing sidewalk strength compared to their use in roads. The challenge, therefore, is to ensure that the subgrade material retains requisite strength while remaining resilient to moisture content variations. Wicking geotextiles, deployed as reinforcement layers between the subgrade and base layers, offer a promising solution for concurrently strengthening and mitigating water-induced damage. In summary, while many studies have validated the drainage capabilities of wicking geotextile fabrics in road contexts, current sidewalk drainage design methods still lack direct applications of wicking geotextiles for enhanced permeable base drainage, and there is a dearth of quantitative analyses focused on leveraging wicking geotextiles to improve the resilience modulus of functional sidewalk bases.

While the aforementioned studies have significantly contributed to our understanding of wicking geotextiles, these studies are mostly based on paved road. The performance of the wicking geotextile-stabilized base under a permeable pavement or paving bricks, where base layer moisture fluctuations are significant, is not well studied, utilizing a wicking geotextile-stabilized base layer. Addressing this gap, the current study undertakes a field experiment to assess the efficacy of a wicking geotextile-stabilized base in a permeable sidewalk. Despite the use of permeable bricks as the surface layer, this year-long experiment offers valuable insights into moisture dynamics within the base layer.

To validate the effectiveness of the permeable sidewalk design, a 1-year field experiment was conducted on a section of permeable sidewalk in the Nanshan District, Shenzhen, China. This experiment included three test sections: 1) an unstabilized base, 2) a base stabilized with a one-directional wicking geotextile, and 3) a base stabilized with a two-directional wicking geotextile. Periodic measurements of the moisture content in these base layers were taken. Additionally, simulated saturation tests were performed on these sections to model the annual water content variation within the base layer. The stabilization effect of the wicking geotextile on the base layer was then analyzed using the relative damage model.

2 Materials

2.1 Wicking geotextiles

This study tested two wicking geotextiles: a one-directional wicking geotextile and a two-directional wicking geotextile. The one-directional wicking geotextile was a commercially ready geosynthetic manufactured by TenCate Geosynthetics that contains wicking fiber in the cross-machine direction. The two-directional wicking geotextile is a prototype material that contains wicking fiber in both machine and cross-machine directions. The properties of the two geotextiles are presented in Table 1.

2.2 Properties of the base material

The foundational material consists of stone fragments, gravel, and sand (A-1-a) according to the AASHTO soil classification system. Figure 2 shows the particle size distribution curve derived from the analyzed soil samples. These samples manifest a coefficient of uniformity (*Cu*) of 17.86, which notably exceeds the standard threshold of 5, and a curvature coefficient (*Cc*) of 1.88, which is within the acceptable range of 1–3. Such indicators suggest a commendable gradation. The maximum dry density determined by the compaction test is 1.87 g/cm^3, while the optimum moisture content is recorded at 10.7%.

To assess the influence of volumetric moisture content on the dynamic, resilient modulus of compacted soil, resilient modulus tests were conducted on soil samples with volumetric moisture contents of 6%, 9%, 12%, 15%, and 18%, respectively. The degree of compaction during the resilient modulus test was maintained at the same level as the pavement base at 95%. The resilient modulus tests were conducted in a dynamic triaxial apparatus according to the Chinese test standard "Design Specification for Highway Subgrade" and the "Procedure for Geotechnical Testing in Highway Engineering" (JTGT-D33-2012, 2012). The prepared soil samples were subjected to a confining pressure of 15 kPa and varying deviator stresses of 10 kPa, 20 kPa, 30 kPa, and 40 kPa. Figure 3A presents the variation of dynamic resilient modulus concerning deviator stress for each moisture content.

This study used the widely applicable NCHEP1-28A model (Barksdale et al., 1997) to predict the dynamic resilient modulus. This model considers the effects of confining stress and shear stress, overcoming the shortcomings of inconsistent dimensions and undefined moduli (Ran et al., 2022). The expression is shown in Eq. (2).

$$M_R = k_1 p_a \left(\frac{\theta}{p_a}\right)^{k_2} \left(\frac{\tau_{oct}}{p_a} + 1\right)^{k_3}, \quad (1)$$

where θ is the confining stress, $\theta = 3\sigma_c + \sigma_d$; τ_{oct} is the octahedral shear stress, $\tau_{oct} = (\sqrt{2}/3)\sigma_d$; p_a is the atmospheric pressure, typically taken as 100 kPa; and k_1, k_2, k_3 is the model parameters, $k_1, k_2 \geq 0, k_3 \leq 0$.

Using Eq. (1), regression analysis was performed on the dynamic triaxial test results to obtain the model parameters k_1, k_2, and k_3 for different moisture contents. Each moisture content group obtained a set of regression model parameter values. Since the equivalent stress levels within the base vary little, the predicted resilient modulus can be calculated based on the recommended equivalent stress levels θ = 70 kPa and τ_{oct} = 13 kPa (Specification for drainage design of highway, 2012). This calculation yields representative dynamic resilient modulus (M_{Rtyp}) values for each moisture content, as shown below. The relationship curve between representative resilient modulus (M_{Rtyp}) and moisture content is shown in Figure 3B. Numerically, the relationship between moisture content and resilient modulus can be expressed as follows:

$$\begin{aligned} &For\ 6\% \leq \omega < 9\% \quad M_{Rtyp} = -12.3\omega + 230.8, \\ &For\ 9\% \leq \omega < 12\% \quad M_{Rtyp} = -11.3\omega + 225.1, \\ &For\ 12\% \leq \omega < 15\% \quad M_{Rtyp} = -7.1\omega + 170.3, \\ &For\ 15\% \leq \omega < 18\% \quad M_{Rtyp} = -5.6\omega + 148. \end{aligned} \quad (2)$$

3 Test setup

Field experiments were conducted in a designated test section of a permeable pedestrian pathway adjacent to a sidewalk planting strip in the Nanshan District of Shenzhen to evaluate the drainage performance of one-directional and two-directional wicking geotextiles (Figure 4).

10.3389/fbuil.2024.1333937

TABLE 1 Geotextile properties.

Property		Test method	Unit		Value	
One-directional wicking geotextile[a]						
Tensile modulus @ 2% strain (CD)		ASTM D4595 (ASTM 2017a)	kN/m		657	-
Permittivity		ASTM D4491 (ASTM 2017b)	S^{-1}		0.24	-
Flowrate		ASTM D4491 (ASTM 2017b)	L/min/m		611	-
Pore size (O50)		ASTM D6767 (ASTM 2016b)	μm		85	-
Pore size (095)		ASTM D6767 (ASTM 2016b)	μm		195	-
Apparent opening size (AOS)		ASTM D4751 (ASTM 2016a)	mm		0.43	-
Wet front movement (24 min)		ASTM C1559 (ASTM 2015)	in	-	60 (vertical direction)	
Wet front movement (983 min) zero gradient		ASTM C1559 (ASTM 2015)	in	-	73.3 (horizontal direction)	
Two-directional wicking geotextile[b]						
Tensile strength at 2% strain	MD	ISO 10319	kN/m		20	
Tensile strength at 2% strain	CD	ISO 10319	kN/m		20	
Tensile strength at 5% strain	MD	ISO 10319	kN/m		50	
Tensile strength at 5% strain	CD	ISO 10319	kN/m		50	
CBR puncture strength		ISO 12236	kN		9	
Grab strength	MD	ASTM D4632	N		2000	
Grab strength	CD	ASTM D4632	N		2000	
Tear strength	MD	ASTM D4533	N		750	
Tear strength	CD	ASTM D4533	N		750	
UV resistance[1]		EN 12224	% retained		90	
G rating[2]		Austroads	-		7,000	
Hydraulic						
Pore size, O_{90}		ISO 12956	mm		0.30	
Water permeability, Q_{50}		ISO 11058	$l/m^2/min$		1,500	

CD, cross-machine direction.
[a]Data from TenCate (2015).
[b]Data provided by TenCate.

1. The sidewalk excavation dimensions were 3 m × 2 m, while the sidewalk planting strip excavation measured 3 m × 1 m. The base was excavated to a depth of 20 cm. The test section was divided into three experimental groups noted as "O" for one-directional, T for two-directional, and C for control, each of dimension 1 m × 3 m.
2. Subsequently, the wicking geotextiles were smoothly laid over the subgrade, starting from the pedestrian pathway, and extended into the sidewalk planting strip. The three experimental groups were arranged from right to left, comprising the two-directional wicking geotextile, the one-directional wicking geotextile, and the control group without geotextile serving as the control group.
3. After the placement of the geotextile, the 200 mm base layer was backfilled and compacted. During the backfilling of the base layer, moisture content sensors were installed at a depth of 150 mm (i.e., 50 mm above the subgrade surface). Along the transverse axis of the three experimental groups, moisture content sensors were installed at a lateral spacing of 1 m and a longitudinal spacing of 0.5 m as depicted in Figure 4. The other end of the sensor cable was extended into a waterproof box positioned in the center of the sidewalk planting strip.
4. The aggregate base was compacted to a degree of compaction of 95% based on ASTM D1556-90. Finally, the permeable paving bricks used in this project primarily consist of refined sand mixed with cementitious materials. Pressed and solidified at room temperature, these bricks are characterized by exceptional permeability and efficient water drainage capabilities. They are designed with a dense surface that effectively prevents the clogging of pores by mud, ash, and other fine particles, thus facilitating easy cleaning and maintenance while maintaining consistent permeability. Furthermore, the bricks demonstrate high strength, wear resistance, and weather resistance, ensuring their durability under various environmental conditions. These bricks were then strategically laid over the designated area.

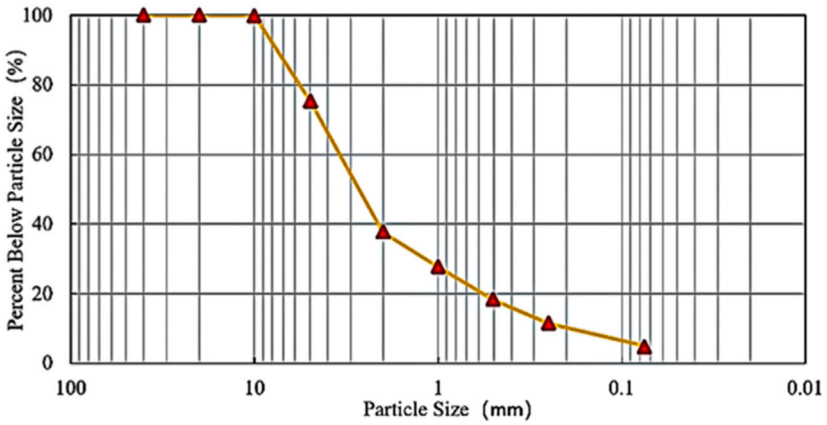

FIGURE 2
Base course material gradation curve.

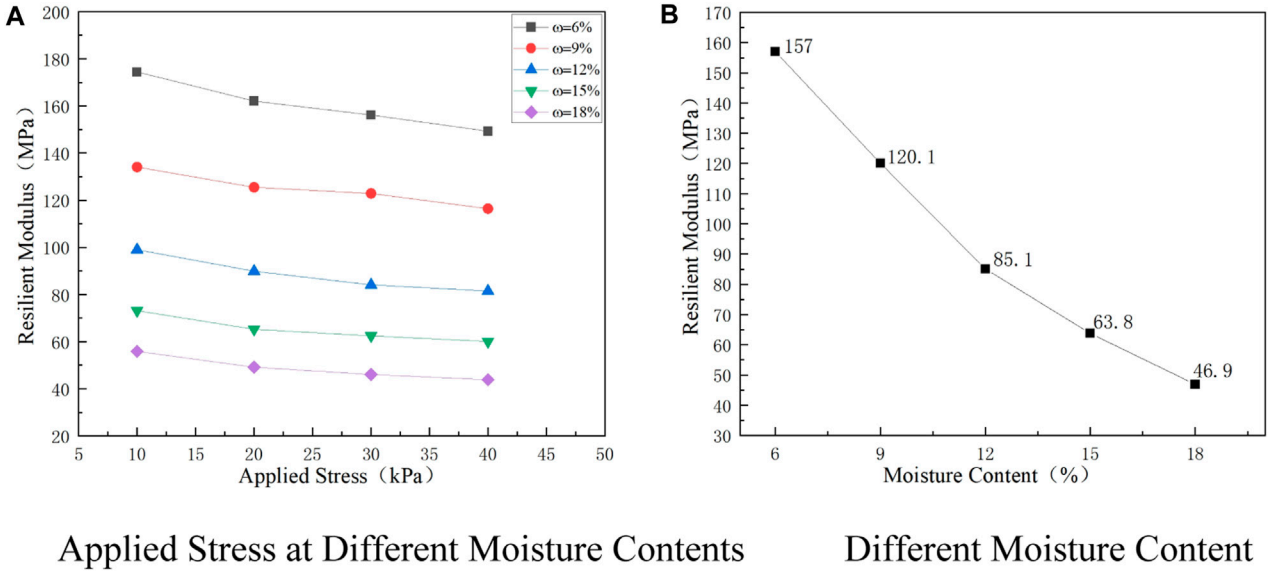

FIGURE 3
Variation of dynamic resilient modulus. **(A)** Applied stress at different moisture contents. **(B)** Different moisture contents.

5. Once the pedestrian walkway was reopened, the sensors were connected to the data acquisition device to commence the collection of moisture content data. However, due to the limitation of battery life and lack of power source, continuous recording over an extended period was not feasible. As a result, data collection from the test sections was carried out at an average interval of 7 days, and the recording period spanned 1 year, from 4 December 2020 to 21 December 2021.
6. A simulated rainfall saturation experiment was conducted over the test groups at the end of the recording period to observe the moisture content change from saturated to unsaturated. During the simulated rainfall experiment, the data acquisition system recorded the water content of the base in 60-s intervals. A water truck was brought in to spread water over the permeable sidewalk until the moisture content of the base layer no longer increased. At this moment, the base is considered saturated. The base layer is then allowed to drain over a period of 20 days, during which the water content of the base is continuously monitored and recorded.

4 Test results and discussion

4.1 Introduction of geotextile configurations and general observations

Figure 5A illustrates the average recorded moisture content of the base layer at a 7-day interval. Three different configurations were compared: the one-directional wicking geotextile (“O”), two-directional wicking geotextile (“T”), and control group (“C”).

10.3389/fbuil.2024.1333937

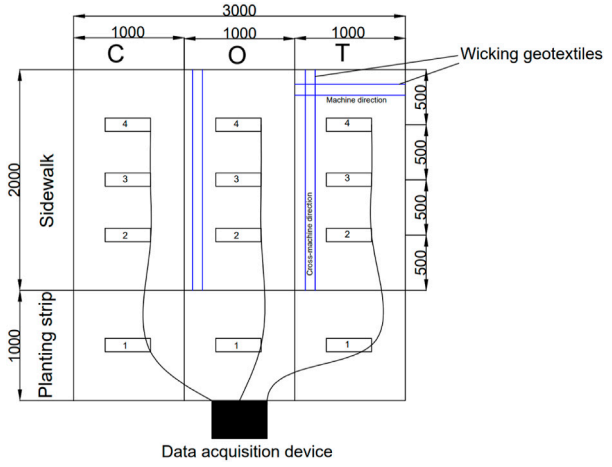

FIGURE 4
Layout of moisture content sensors (unit: mm).

The C line, which represents the control sample without the application of wicking geotextiles, shows considerable variability in moisture content. It peaks significantly around day 180 and again after day 300, suggesting seasonal influences or external factors that contribute to moisture increase. The O line, indicative of a sample with a one-directional wicking geotextile, generally follows the trend of the control but with a notable reduction in moisture content. This suggests that the one-directional wicking is effective in reducing moisture but does not eliminate variability altogether. The T line, representing the two-directional wicking geotextile condition, shows the most stable trend with the lowest moisture content throughout the year. The reduced variability and lower peaks imply that two-directional wicking geotextiles are more effective in maintaining a consistent and lower moisture content. The moisture content trends in all three test sections exhibit similarities. It is evident that the base layer reinforced with wicking geotextiles consistently maintained lower average moisture content throughout the year compared to the control layer.

4.2 Analysis of trends and moisture content variability

The fluctuation of moisture content was caused by rainfall events. A subsequent data point presented a lower water content, indicating over the period, water was drained from the road section. On the other hand, if the subsequent data point presented a higher water content, a rainfall event occurred which resulted in moisture content increase over the period. The lines for O and T, which represent the test sections with wicking geotextiles, generally follow a similar trend but with distinct differences from the control line C.

4.3 Annual average moisture content and comparative analysis

Overall, the annual average moisture content of the geotextile-reinforced base layer remains around 10%. The

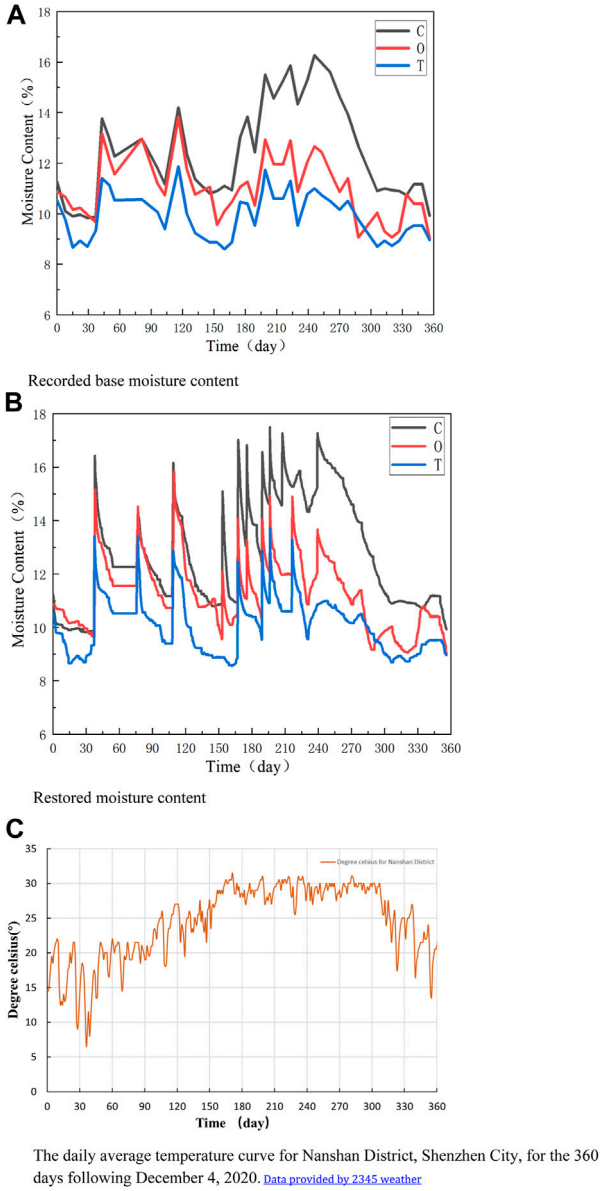

FIGURE 5
Moisture content variation curves of different wicking geosynthetic fabrics over 1 year and the daily average temperature curve. **(A)** Recorded base moisture content. **(B)** Restored moisture content. **(C)** Daily average temperature curve for Nanshan District, Shenzhen City, for the 360 days following December 4, 2020.

one-directional wicking geotextile achieves approximately 11% moisture content, the two-directional wicking geotextile maintains around 9.9%, and the control base layer exhibits an average moisture content of approximately 12.5%. Compared to the initial moisture content, over the duration of 1 year, the two-directional wicking geotextile reduces the moisture content of the base layer by 2.6%, while the one-directional wicking geotextile reduces it by 1.5%. The moisture content of the two-directional wicking geotextile-reinforced layer is 1.1% lower than that of the one-directional wicking geotextile-reinforced layer. In conclusion, using wicking geotextiles in the base layer significantly enhances drainage performance. Among the two

types of wicking geotextiles tested, the two-directional wicking geotextile exhibits superior drainage performance compared to the one-directional wicking geotextile.

4.4 Specific observations of the one-directional wicking geotextile

During the first half of the year, the average moisture content of the base layer reinforced with the one-directional wicking geotextile is similar to that of the control base layer. However, in the second half of the year, it gradually approaches the moisture content of the two-directional wicking geotextile-reinforced layer, showing a decrease of 2.4% compared to the control base layer. This suggests that the drainage capacity of the one-directional wicking geotextile is weaker in the first half of the year while improving in the latter half of the year.

Rainfall frequency could be the major contributor to the altered drainage performance of the one-directional wicking geotextile. From Figure 5B, for the first 150 days, the water contents in the one-directional wicking geotextile section and the control sections are similar, as rainfall frequency was around once a month. However, as rainfall frequency increases, during days 150–250, the water content in the control section gradually increases, while that of the one-directional wicking geotextile section is maintained at a relatively low level, similar to that of the two-directional section. The moisture content increase between days 150 and 250 in the control section suggests an insufficient drainage capacity under frequent rainfall. On the other hand, the one-directional wicking geotextile is more effective in removing water from the base layer when rainfall occurs more frequently. By comparison, the two-directional wicking geotextile maintained the moisture content at a relatively low level, indicating the additional wicking fiber improves drainage.

Temperature could be the second contributor to the altered drainage capacity of the one-directional wicking geotextile: the lower temperatures in the first half of the year result in poorer drainage performance, while higher temperatures in the second half of the year contribute to better drainage performance. The temperature profile over the test period is depicted in Figure 5C, indicating that below 25°C, the one-directional geotextile does not exhibit its full drainage capacity during the initial 150 days. Conversely, during the 150–300-day period when temperatures exceed 25°C, a notable variance in moisture content is observed between the one-directional geotextile and the control group. After 330 days, as temperatures fall back below 25°C, a rainfall event elevated the moisture levels in the one-directional geotextile to nearly match those of the control group. This finding aligns with Liu et al.'s conclusion based on field experiments, which states that due to the fast evaporation rate at high temperatures and the soil's increased hydraulic conductivity, the wicking geotextile can reduce VWCs in the aggregate base more at high temperatures than at low temperatures (Liu et al., 2022). This effect can also be related to the unique deep-groove fiber design of one-directional wicking geotextiles, a feature not present in their two-directional counterparts, which requires additional investigation.

4.5 Comparison and effectiveness of different wicking geotextiles

The red (O) and blue (T) lines, after an initial period, consistently remain below the black (C) line, suggesting that both one-directional and two-directional wicking geotextiles reduce moisture content in the base layer compared to the control without the geotextile. The blue line (T) for the two-directional wicking geotextile often lies below the red line (O), indicating that the two-directional wicking geotextile is more effective in reducing moisture content than the one-directional variant.

4.6 Seasonal variability and its impact

The peaks and troughs in the graph indicate seasonal variations in moisture content, with potential higher moisture content during wet seasons and lower moisture content during dry seasons. This seasonal effect appears to be mitigated by the use of wicking geotextiles, as seen by the reduced amplitude of fluctuations in O and T compared to C.

The degree of moisture content variation can be difficult to capture, especially for the case where the moisture content is measured with intervals as this study. To tackle this problem, an analytical method was proposed in this study. The method restores the daily moisture content of the base layer according to the base drainage characteristic curve and evaluates the improvement in the resilient modulus due to wicking geotextiles' drainage effect. The process involves the following steps:

1) Quantifying the post-rainfall moisture content variation rate: Saturated–unsaturated rainfall tests are conducted to determine the rate at which the moisture content changes after rainfall events.
2) Estimating the daily moisture content: By combining periodic measurements of moisture content and the post-rainfall moisture content variation rate, it becomes possible to estimate the daily moisture content over a year.
3) Developing a moisture content-resilient modulus function model: This step involves conducting dynamic triaxial tests and employing the NCHEP1-28A equation to establish a relationship between the moisture content and the resilient modulus of the base layer.
4) Applying the AASHTO 1993 design specification's relative damage model (American Association of State Highway and Transportation Officials, 1993): The AASHTO 1993 model, which considers relative damage with respect to resilient modulus, is employed to calculate the annual equivalent resilient modulus. This model takes into account the cumulative damage experienced by the base layer over time.
5) Evaluating the improvement of the base layer's resilient modulus using wicking geotextiles: A comparative analysis is performed by assessing the annual equivalent resilient modulus of three scenarios: the control base layer, one-directional wicking geotextile-reinforced layer, and two-directional wicking geotextile-reinforced layer. This enables the quantification of the enhancement in the resilient modulus achieved through the implementation of wicking geotextiles.

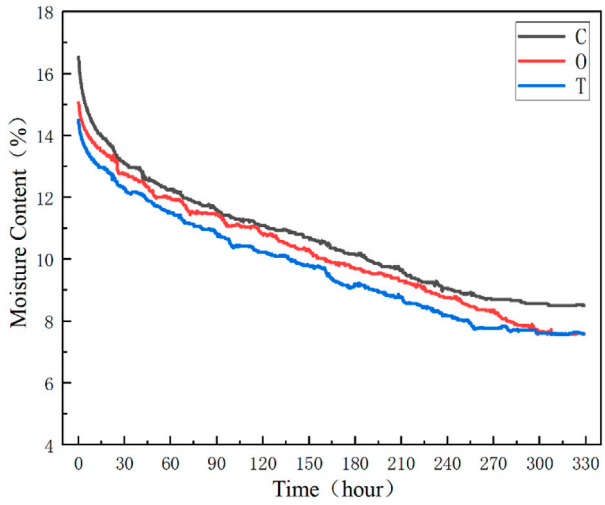

FIGURE 6
Base drainage characteristic curve based on the simulated rainfall saturation test.

4.6.1 Restoration of daily moisture content (steps 1 and 2)

In practical engineering applications, continuously and uninterruptedly monitoring the moisture content in road base layers poses a significant challenge. In this study, the moisture content of the base layer was measured at intervals ranging from 7 to 10 days. After rainfall, the base layer's moisture content typically exhibits an initial rapid increase, followed by a swift decrease within a brief period, and, subsequently, a gradual decline. The variation rate of moisture content during this cycle is notably variable, rendering linear interpolation inadequate for accurately estimating daily moisture content.

In this chapter, a novel method is introduced to estimate the daily moisture content of the base layer. This method is predicated on the assumption that the drainage rate of a base layer under unsaturated conditions relies exclusively on its moisture content and the drainage efficacy facilitated by wicking geotextile. Moreover, it is posited that the number of rainfall events does not influence the unsaturated flow characteristics of the base layer. In essence, the decline in the moisture content of a base layer consistently adheres to a specific drainage characteristic curve, which is ascertainable through a simulated rainfall saturation experiment. Figure 6 illustrates this base layer drainage characteristic curve, derived from experimental results of the simulated experiment. Notably, the curve's duration spans approximately 14 days, exceeding the intervals of field moisture content recording. This drainage characteristic curve effectively tracks the moisture content's reduction from roughly 17% to 8%.

Subsequently, the annual recorded moisture content from Figure 5A was divided into segments based on adjacent moisture content records with the duration of Δt. Each segment had an initial recorded moisture content denoted as ω_i and a final recorded moisture content denoted as ω_f. The case of $\omega_i < \omega_f$ indicates an increase in base moisture content caused by rainfall, and the restoration process followed the ascending phase method. Conversely, the case of $\omega_i > \omega_f$ indicates a decrease in base moisture content, and the restoration process followed the descending phase method. Based on the initial or final recorded moisture content, a series of values of moisture content on the base drainage characteristic curve were used to fill the gap between the initial and final moisture content.

4.6.1.1 Ascending section restoration

The ascending phase ($\omega_i<\omega_f$) of the base moisture content is restored by utilizing the reverse inference of the drainage characteristic curve. Two restoration methods are defined based on the field recording time interval (Δt) and the duration (Δt_1) from ω_m to ω_f on the drainage characteristic curve: $\Delta t_1 \geq \Delta t$ and $\Delta t_1 < \Delta t$, corresponding to Figures 7A,B, respectively.

When $\Delta t_1 \geq \Delta t$, it indicates a rainfall event occurred immediately after the beginning of the segment, where the

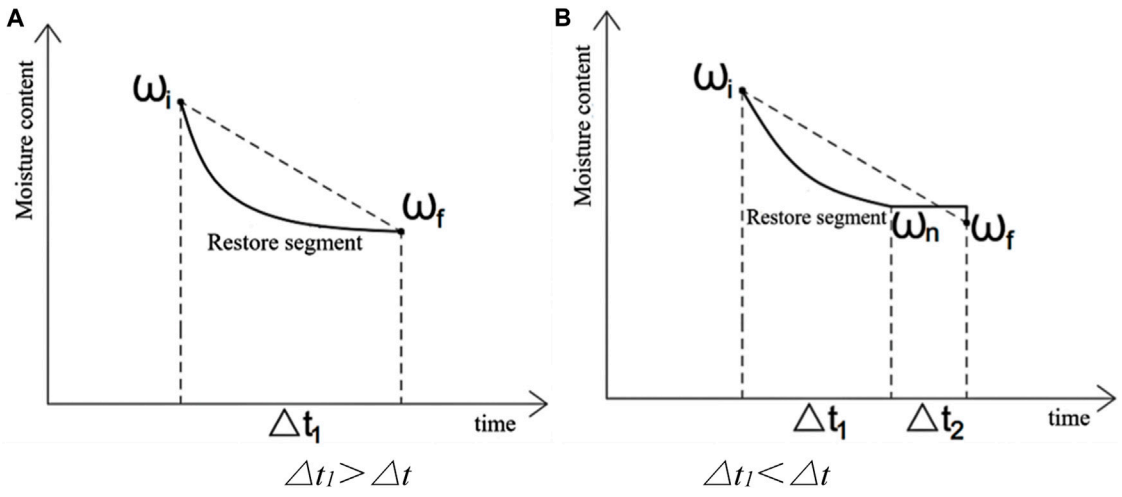

FIGURE 7
Moisture content reduction model during the drying phase. **(A)** $\Delta t1>\Delta t$. **(B)** $\Delta t1<\Delta t$.

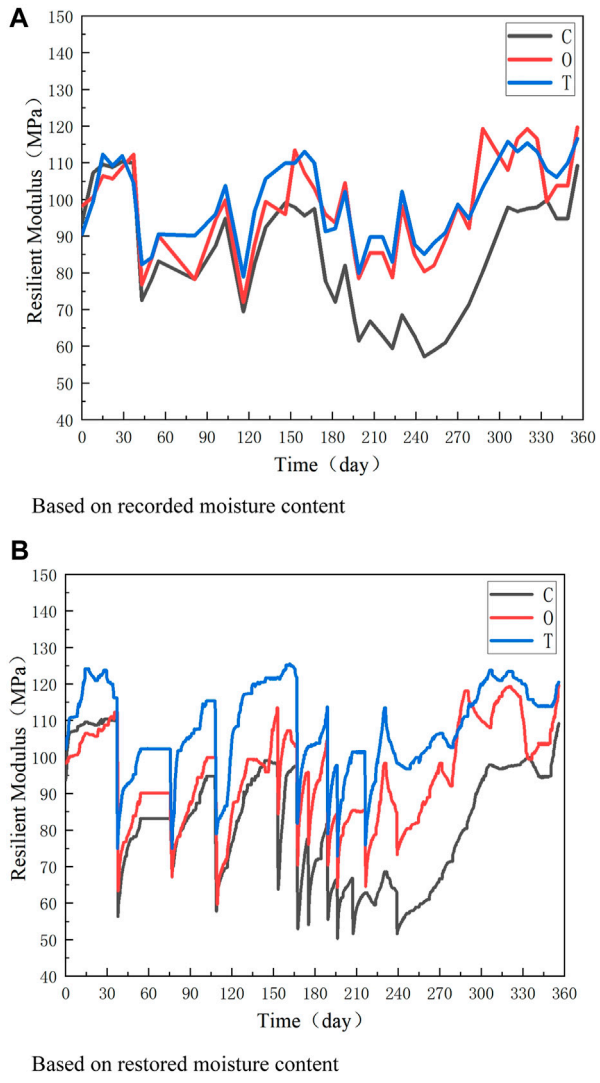

FIGURE 8
Variation of the annual representative resilient modulus over time. **(A)** Based on the recorded moisture content. **(B)** Based on the restored moisture content.

base layer water content increased from ω_i to ω_m in a relatively short time. Then, the value of ω_m can be determined by the duration Δt, the final moisture content value ω_f, and the drainage characteristic curve. Since the period of base moisture content increase caused by rainfall can be disregarded over the entire year, the influence of the ascending phase time is neglected. Hence, the initial moisture content ω_i at the beginning is directly connected to the peak moisture content ω_m, forming the restoration segment depicted in Figure 7A.

When $\Delta t_1 < \Delta t$, it indicates a rainfall event occurred between the beginning and end of the segment. The segment Δt is divided into two subsegments: Δt_1 and Δt_2. Δt_1 represents a period following a rainfall where the base moisture content decreases, and Δt_2 denotes the time interval between the rainfall and the start of the segment. The restoration process for subsegment Δt_1 follows the same procedure as described previously, where ω_f and the drainage characteristic curve were used to determine the duration of Δt_1. The moisture content ω_m at the beginning of subsegment Δt_1 equals to the peak value of the drainage characteristic curve. Considering that the base moisture content increase caused by rainfall can be neglected over the entire year, at the end of Δt_2, the initial moisture content ω_i abruptly increases to ω_m. Then, by assuming that Δt_2 was the later stage of the drainage phase, where the moisture content reaches a relatively stable state, the moisture content remains unchanged during the period of subsegment Δt_2. Thus, the base moisture content over subsegment Δt_2 remained as ω_i, as demonstrated in Figure 7B.

4.6.1.2 Descending section restoration

Due to the relatively short interval, the descending phase ($\omega_i > \omega_f$) typically indicates a phase where no rainfall event occurred and the base layer is in a drying process. Two restoration methods are defined based on the field recording time interval (Δt) and the duration (Δt_1) from ω_i to ω_n on the drainage characteristic curve: $\Delta t_1 \geq \Delta t$ and $\Delta t_1 < \Delta t$, corresponding to Figures 8A,B, respectively.

When $\Delta t_1 \geq \Delta t$, it indicates the actual drainage speed is higher than that being represented by the drainage characteristic curve. In this case, the restored moisture content of the segment is obtained by scaling the section of the drainage characteristic curve between ω_i and ω_f, as presented in Figure 8A.

When $\Delta t_1 < \Delta t$, the segment was further divided into two subsegments Δt_1 and Δt_2. The moisture content during Δt_1 was determined by initial moisture content ω_i and the drainage characteristic curve, where the lowest moisture content was ω_n. During the base moisture content decrease process, the rate of change gradually decreases until it reaches zero. Therefore, once the moisture content decreases to ω_n, the moisture content during subsegment Δt_2 can be considered unchanged (where $\omega_n \approx \omega_f$). This forms the final restoration segment, as Figure 8B illustrates.

Based on the aforementioned methods, the restored daily moisture content is presented in Figure 5B. Since the recording time interval (Δt) is typically longer than the time duration (Δt_1) between ω_i and ω_f on the drainage characteristic curve, the restored moisture content predominantly resembles the patterns depicted in Figure 7B and Figure 8B.

4.7 Calculation of the annual equivalent resilient modulus (steps 3 and 4)

The concept of the equivalent resilient modulus was introduced in the "AASHTO 1993 Road Design Specifications" to account for the cyclical changes in base moisture content due to seasonal variations, affecting the base soil's resilient modulus (American Association of State Highway and Transportation Officials, 1993). Initially proposed by Guo (2017) under the guidance of Dr. Jie Han, the equivalent resilient modulus quantifies the average cumulative annual damage from road traffic and is calculated as a weighted average. The time period is segmented into equal intervals to ascertain the base soil sample's equivalent resilient modulus over a specified duration. For each interval, the average resilient modulus is computed, and the relative damage (u_f) is determined using Eq. (3). Substituting u_f into Eq. (4) yields the average relative damage ($\overline{u_f}$). The equivalent resilient modulus is then calculated for that period.

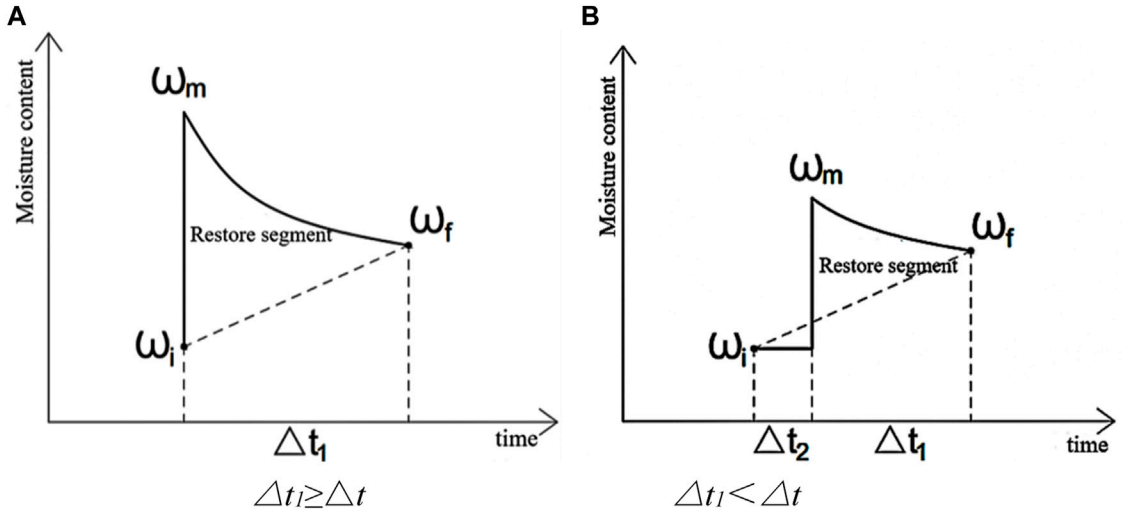

FIGURE 9
Model of ascending section restoration for moisture content. **(A)** △t1≥△t. **(B)** △t1<△t.

$$u_f = 1.18 \times 10^8 \times M_r^{-2.32}, \quad (3)$$

$$\overline{u_f} = \frac{u_f}{n}, \quad (4)$$

$$\overline{M_R} = \left(\frac{1.18 \times 10^8}{\overline{u_f}} \right)^{\frac{1}{2.32}}, \quad (5)$$

where $\overline{u_f}$ is the average relative damage; u_f is the relative damage; M_r is the resilient modulus for each moisture content; $\overline{M_R}$ is the equivalent resilient modulus.

In this study, the resilient modulus of the base layer can be calculated based on the recorded base moisture content or restored daily moisture content. In the case that recorded moisture contents were used, the average monthly water content was calculated based on recorded values, and then, the monthly resilient modulus was calculated based on the average monthly moisture content with Eq. (5). The 1-year equivalent resilient modulus based on the recorded moisture content, $\overline{Mr_{month}}$, is calculated with the number of studied segments of 12, and the duration of each period was 1 month. In the case that restored moisture contents were used, the daily moisture content was used to calculate the daily resilient modulus. The equivalent resilient modulus over a year based on the restored moisture content, $\overline{Mr_{day}}$, is calculated with the number of studied segments of 365. In other words, the $\overline{Mr_{month}}$ is calculated based on only the recorded moisture content in the study period of month, while the $\overline{Mr_{day}}$ is calculated with the restored moisture content in the study period of day.

Figure 9 presents the recorded and restored resilient modulus calculated based on recorded and restored moisture contents. The $\overline{Mr_{day}}$, based on restored moisture contents, for control, one-directional wicking geotextile, and two-directional wicking geotextile sections was 82.5 MPa, 94.9 MPa, and 107.8 MPa, respectively. The $\overline{Mr_{month}}$ for control, one-directional wicking geotextile, and two-directional wicking geotextile sections was 77.25 MPa, 93.1 MPa, and 106.6 MPa, respectively.

The $\overline{Mr_{day}}$, based on recorded moisture contents, for control, one-directional wicking geotextile, and two-directional wicking geotextile sections was 82.5 MPa, 94.9 MPa, and 107.8 MPa, respectively. The $\overline{Mr_{month}}$ for control, one-directional wicking geotextile, and two-directional wicking geotextile sections was 77.25 MPa, 93.1 MPa, and 106.6 MPa, respectively.

4.8 Assessment of the increased resilient modulus by the wicking geotextile (step 5)

In comparison, the restored moisture content curves (Figure 5B) more closely resembled the moisture content in real life, offering a clearer view of the rapid changes in moisture levels, which could be crucial for understanding the dynamics of water movement within the base layer. The equivalent resilient modulus showed a difference too. The equivalent resilient modulus calculated based on the restored daily moisture content $\overline{Mr_{day}}$ is 1.8% lower, 1.3% lower, and 8.5% higher than the equivalent resilient modulus calculated based on the recorded moisture content ($\overline{Mr_{month}}$), respectively.

According to recorded daily moisture content, the $\overline{Mr_{month}}$ of the one-directional geotextile- and two-directional geotextile-reinforced section is 14.7 MPa (2132.21 PSI) and 18.9 MPa (2741 PSI) higher than that of the control section, which presents a 18.74% and 24.09% increase in resilient modulus, respectively. The $\overline{Mr_{month}}$ of the two-directional geotextile-reinforced base is 4.2 MPa (608.74 PSI) higher than that of the one-directional geotextile-reinforced section, representing a 4.51% increase. According to the restored daily moisture content, the $\overline{Mr_{day}}$ of the one-directional geotextile- and two-directional geotextile-reinforced section is 14.9 MPa (2161.5 PSI) and 28.6 MPa (4144.9 PSI) higher than that of the control section, which presents a 19.35% and 37.11% increase in resilient modulus, respectively. The $\overline{Mr_{day}}$ of the two-directional geotextile-reinforced base is 13.67 MPa (1983.4 PSI) higher than that of the one-directional geotextile-reinforced section,

representing a 14.88% increase. Overall, the moisture content reduction effect of the wicking geotextile significantly improved the resilient modulus of the base layer. It is to be noted that the relative damage model was designed to evaluate the soil strength for pavement applications, and however, the authors believe that the analytical process can be applicable to most of the roadways.

5 Conclusion

This study involved a year-long field experiment on permeable sidewalks, where three test sections were compared: an unreinforced base, a base reinforced with a one-directional wicking geotextile, and a base reinforced with a two-directional wicking geotextile. The moisture content in these sections was meticulously recorded and analyzed. The study evaluated the efficacy of wicking geotextiles in enhancing base drainage and resilient modulus. From the findings, the following conclusions were drawn:

(1) The geotextile-reinforced base layers consistently showed an average moisture content of approximately 10%. Specifically, the base layer with the one-directional wicking geotextile showed an average moisture content of approximately 11%, while the two-directional wicking geotextile maintained an average moisture content of approximately 9.9%. In contrast, the control base layer exhibited an average moisture content of approximately 12.5%. The one-directional geotextile-reinforced base layer displayed moisture content fluctuations roughly between 9% and 13%, with periodic variations influenced by seasonal and rainfall patterns. Conversely, the two-directional geotextile-reinforced base layer demonstrated a relatively stable and lower fluctuation range, mostly between 9% and 11%, indicative of superior water regulation capabilities. The control group, lacking reinforcement, showed the highest fluctuation, ranging from 10% to 16%, particularly during high-rainfall periods. These results underscore the advantages of geotextile reinforcement in maintaining optimal moisture levels. The two-directional wicking geotextile, in particular, excelled in keeping the base layer dry with minimal fluctuation, suggesting its greater efficiency in moisture expulsion under various climatic conditions.

(2) The inclusion of wicking geotextiles significantly enhances the resilient modulus of the permeable base, considering solely the impact of water content. Specifically, one-directional wicking geotextiles increased the annual equivalent resilient modulus by 19.35%, while two-directional geotextiles achieved an increase of 37.11%, based on the restored moisture content. This underscores the substantial role of wicking geotextiles in improving the base layer's mechanical properties, particularly the resilient modulus, a key metric of structural integrity. The beneficial effect is quantitatively evident over a year-long period. For instance, bases reinforced with one-directional wicking geotextiles exhibited an increase in the annual equivalent resilient modulus to 91.9 MPa from the original 77.0 MPa, marking a 19.35% enhancement. More impressive is the improvement with two-directional wicking geotextiles, where the resilient modulus surged by 37.11%–105.6 MPa from the baseline of 77.0 MPa. These figures, derived from comprehensive annual monitoring, highlight the superior performance of two-directional geotextiles in moisture regulation and base stabilization. The corresponding graphical data, as depicted in Figure 1 and Figure 2, align with these findings. Figure 1 shows the resilient modulus calculated from the directly measured moisture content, while Figure 2 presents the modulus after applying our moisture restoration technique. The noticeable differences between these figures not only confirm the effectiveness of two-directional geotextiles in adjusting moisture levels but also indicate their potential in reducing moisture-related degradation in permeable bases. This empirically grounded understanding of the moisture–modulus relationship is critical in developing more resilient infrastructure that can withstand environmental fluctuations. Future research could delve into the specific behaviors of these geotextiles under various climatic conditions and assess their long-term impact on pavement durability and maintenance efficiency. Such in-depth investigations could further clarify the influence of geotextile orientation on moisture management, potentially guiding optimized designs for maximum pavement longevity.

(3) The equivalent resilient modulus calculated based on the recorded and restored moisture content presented a large difference for the two-directional wicking geotextile, where $\overline{Mr_{day}}$ is 8.5% higher than $\overline{Mr_{month}}$. This variance is quantified by a marked 8.5% higher daily average resilient modulus $\overline{Mr_{day}}$ compared to the $\overline{Mr_{month}}$ after adjusting for moisture content. This discrepancy underscores the dynamic interaction between geotextile properties and environmental factors on a daily basis, as opposed to a broader monthly average which may dilute such interactions. Such a difference suggests that the two-directional wicking geotextile's moisture regulation capabilities are not only highly effective but also responsive to daily environmental fluctuations, which may include variations in temperature, precipitation, and humidity. The daily restored moisture content, facilitated by the two-directional wicking action, enhances the base's resilience modulus, leading to a more robust and durable infrastructure. This insight is particularly valuable for the design and implementation of sidewalk foundation stabilization in regions experiencing significant precipitation variability. It implies that the two-directional geotextiles are particularly adept at managing the micro-scale moisture dynamics that can significantly influence the mechanical performance of the base layer. These findings may encourage the adoption of two-directional wicking geotextiles in the design of permeable bases to exploit their superior moisture management for enhancing the durability and performance of pavement structures.

(4) The drainage efficiency of one-directional wicking geotextiles appears to be influenced by environmental factors such as temperature and rainfall frequency. Higher temperatures and more frequent rainfall events seem to enhance their performance. This effect is likely due to the unique deep-

groove fiber design of one-directional wicking geotextiles, a feature not present in their two-directional counterparts. Elevated temperatures may increase thermodynamic activity within these deep grooves, thereby improving the capillary action essential for effective moisture movement. Similarly, frequent rainfall allows these specialized fibers to channel water more efficiently, ensuring consistent drainage from the base layer. This distinctive fiber design might account for the varied performance observed throughout different times of the year. In warmer periods with regular rainfall, the deep-groove fibers of one-directional wicking geotextiles potentially exhibit a more effective capillary effect compared to the flatter fibers in two-directional varieties. This results in enhanced moisture management under such climatic conditions, thereby reducing the risk of saturation and related damage to the base layer. Consequently, the incorporation of deep-groove fibers could be a crucial element in the design of one-directional wicking geotextiles, especially in environments with diverse temperature ranges and varying rainfall patterns. Future research should further investigate the relationship between fiber design, environmental conditions, and drainage efficacy. Such studies could pave the way for more specialized and effective applications of geotextile materials in various civil and environmental engineering projects, optimizing their use based on climatic variables.

Data availability statement

The raw data supporting the conclusion of this article will be made available by the authors, without undue reservation.

Author contributions

XX: writing–original draft, writing–review and editing, funding acquisition, and supervision. LL: writing–original draft, data curation, investigation, and writing–review and editing. GY: writing–review and editing and funding acquisition. ZL: writing–review and editing and resources. YT: writing–review and editing and resources. JC: writing–review and editing. WW: writing–review and editing, investigation, validation, and writing–original draft. AC: writing–original draft, writing–review and editing, data curation, and formal analysis. JG: conceptualization, methodology, and writing–original draft.

Funding

The authors declare that financial support was received for the research, authorship, and/or publication of this article. The research presented in this paper was sponsored by the National Science Foundation of China (No. 42002267), Shenzhen Natural Science Fund (the Stable Support Plan Program 20200812152953002), and Shenzhen High-End Talent Research Start-Up Project (Project Number 20220082).

Acknowledgments

The authors would like to express their gratitude toward the Transportation Committee of Nanshan District, Shenzhen, for their support in arranging the test site.

Conflict of interest

Author JC was employed by TenCate Industrial Zhuhai Co.

The remaining authors declare that the research was conducted in the absence of any commercial or financial relationships that could be construed as a potential conflict of interest.

Publisher's note

References

AASHTO (1993). AASHTO soil classification system. Available at: https://transportation.org/technical-training-solutions/wp-content/uploads/sites/64/2023/02/AT-TC3CN025-18-T1-JA021.pdf.

Alvarenga, C., Parisa, H. A., and Michael, T. H. (2021). "Moisture and soil strength monitoring of a railway embankment remediated with wicking geotextile," in MATEC Web of Conferences (Les Ulis, France: EDP Sciences). 337, 03001.

American Association of State Highway and Transportation Officials (1993). *Aashto guide for design of pavement structures*. Washington, DC: American Association of State Highway and Transporation Officials.

ASTM International (1990). *Astm D 1556-90: standard test method for density and unit weight of soil in place by the sand-cone method*. West Conshohocken, PA: ASTM International.

Bai, M., Liu, Z., Zhang, S., Liu, F., Lu, L., and Zhang, J. (2021). Experimental study on the effect of fabric parameter on drainage performance of wicking geotextile. *Fibers Polym.* 22 (7), 2044–2051. doi:10.1007/s12221-021-0359-5

Barksdale, R. D., Lago Alba, J. A., Khosla, N. P., Kim, R., Lambe, P. C., and Rahman, M. S. (1997). *NCHRP web doc 14 laboratory determination of resilient modulus for flexible pavement design: final report*. Washington, DC: The National Academies Press. doi:10.17226/6353

Bathurst, R. J., Ho, A. F., and Siemens, G. (2007). A column apparatus for investigation of 1-D unsaturated-saturated response of sand-geotextile systems. *Geotechnical Test. J.* 30 (6), 433–441. doi:10.1520/GTJ100954

Chen, J., Liu, Y., Gitau, M. W., Engel, B. A., Flanagan, D. C., and Harbor, J. M. (2019). Evaluation of the effectiveness of green infrastructure on hydrology and water quality in a combined sewer overflow community. *Sci. Total Environ.* 665, 69–79. doi:10.1016/j.scitotenv.2019.01.416

Coble, A. A., Wymore, A. S., Shattuck, M. D., Potter, J. D., and McDowell, W. H. (2018). Multiyear trends in solute concentrations and fluxes from a suburban watershed: evaluating effects of 100-Year flood events. *J. Geophys. Res.* 123 (9), 3072–3087. doi:10.1029/2018jg004657

Coseo, P., and Larsen, L. (2019). Accurate characterization of land cover in urban environments: determining the importance of including obscured impervious surfaces in urban heat island models. *Atmosphere* 10 (6), 347. doi:10.3390/atmos10060347

Federal Highway Administration (FHWA) (1992). *Drainage pavement system participant notebook*, 87. Demonstration Project No: FHWA-SA-92-008.

Garcia, E. F., Gallage, C. P. K., and Uchimura, T. (2007). Function of permeable geosynthetics in unsaturated embankments subjected to rainfall infiltration. *Geosynth. Int.* 14 (2), 89–99. doi:10.1680/gein.2007.14.2.89

Guo, J. (2017). Evaluation and design of wicking geotextile for pavement applications. Doctoral dissertation. Lawrence, KS: University of Kansas.

Guo, J., Han, J., Zhang, X., and Li, Z. (2019). Evaluation of moisture reduction in aggregate base by wicking geotextile using soil column tests. *Geotext. Geomembranes* 47 (3), 306–314. doi:10.1016/j.geotexmem.2019.01.014

Guo, J., Wang, F., Zhang, X., and Han, J. (2016). Quantifying water removal rate of a wicking geotextile under controlled temperature and relative humidity. *ASCE J. Mater. Civ. Eng.* 29 (1), 04016181. doi:10.1061/(asce)mt.1943-5533.0001703

Guo, J., Wang, F., Zhang, X., and Han, J. (2017). Quantifying water removal rate of a wicking geotextile under controlled temperature and relative humidity. *J. Mater. Civ. Eng.* 29 (1), 04016181. doi:10.1061/(asce)mt.1943-5533.0001703

Hachem, A. E., and Zornberg, J. G. (2019). Enhanced lateral drainage geotextile to mitigate the effects of moisture migration from a high-water table. *Geo-Congress*, 227–234. doi:10.1061/9780784482124.024

Han, J., and Zhang, X. (2014). *Recent advances in the use of geosynthetics to enhance sustainability of roadways. Invited keynote lecture, conference on advances in civil engineering for sustainable development*. Thailand: Nakhon Ratchasima, 27–29.

Iryo, T., and Rowe, R. K. (2004). Numerical study of infiltration into a soil–geotextile column. *Geosynth. Int.* 11 (5), 377–389. doi:10.1680/gein.11.5.377.53141

Koerner, R. M. (2012). *Designing with geosynthetics*, 1. Xlibris Press: Xlibris Corporation.

Laprade, R. B., and Lostumbo, J. M. (2020). "Enhanced moisture management of pavement systems through capillary suction," in *Geo-congress 2020* (Reston, VA: American Society of Civil Engineers), 587–596.

Li, C., Liu, M., Hu, Y., Shi, T., Qu, X., and Walter, M. T. (2018). Effects of urbanization on direct runoff characteristics in urban functional zones. *Sci. Total Environ.* 643, 301–311. doi:10.1016/j.scitotenv.2018.06.211

Lin, C., and Zhang, X. (2019). "Numerical investigation of a saturated and unsaturated soil-atmosphere model," in Eighth International Conference on Case Histories in Geotechnical Engineering, Reston, VA (American Society of Civil Engineers), 765–772.

Lin, C., and Zhang, X. (2020). "Comparisons of geotextile-water characteristic curves for wicking and non-wicking geotextiles," in *Geo-congress 2020: engineering, monitoring, and management of geotechnical infrastructure* (Reston, VA: American Society of Civil Engineers), 629–636.

Lin, C., Zhang, X., and Han, J. (2019). Comprehensive material characterizations of pavement structure installed with wicking fabrics. *J. Mater. Civ. Eng.* 31 (2), 4018372. doi:10.1061/(asce)mt.1943-5533.0002587

Liu, H., Han, J., Al-Naddaf, M., Parsons, R. L., and Kakrasul, J. I. (2022). Field monitoring of wicking geotextile to reduce soil moisture under a concrete pavement subjected to precipitations and temperature variations. *Geotext. Geomembranes* 50 (5), 1004–1019. doi:10.1016/j.geotexmem.2022.07.001

McCartney, J. S., and Zornberg, J. G. (2010). Effects of infiltration and evaporation on geosynthetic capillary barrier performance. *Can. Geotechnical J.* 47 (11), 1201–1213. doi:10.1139/t10-024

Moore, T. L., Rodak, C. M., Ahmed, F., and Vogel, J. R. (2016). Urban stormwater characterization, control, and treatment. *Water Environ. Res.* 88 (10), 1821–1871. doi:10.2175/106143018x15289915807452

Qin, Z., Fu, H., and Chen, X. (2019). A study on altered granite meso-damage mechanisms due to water invasion-water loss cycles. *Environ. Earth Sci.* 78 (14), 428. doi:10.1007/s12665-019-8426-6

Radfar, A., and Rockaway, T. D. (2016). Captured runoff prediction model by permeable pavements using artificial neural networks. *J. Infrastructure Syst.* 22 (3), 04016007. doi:10.1061/(asce)is.1943-555x.0000284

Ran, W., Wang, J., Li, L., and Chen, H. (2022). Laboratory test and prediction model of dynamic resilient modulus of coarse-grained sulfate saline soil. *J. Hunan Univ. Nat. Sci.* 49 (3), 154–166. doi:10.16339/j.cnki.hdxbzkb.2022036

Reebie Associates, Economic Development Research Group, Carl Martland (2004). *Rail freight solutions to roadway congestion: interim report on transportation trends, road-to-rail diversion and model elements for decision-making (Task 3-4-5-6 Report)*. National Cooperative Highway Research Program (NCHRP).

Shafique, M., and Kim, R. (2017). Green stormwater infrastructure with low impact development concept: a review of current research. *Desalination Water Treat.* 83, 16–29. doi:10.5004/dwt.2017.20981

Shakya, S., Tamaddun, K. A., Stephen, H., and Ahmad, S. (2019). "Urban runoff and pollutant reduction by retrofitting green infrastructure in stormwater management system," in *World environmental and water resources congress 2019: water, wastewater, and stormwater; urban water resources; and municipal water infrastructure* (Reston, VA: American Society of Civil Engineers), 93–104.

Specification for drainage design of highway (2012). *Specification for drainage design of highway*. JTGT-D33-2012. Beijing: Ministry of Transport of the People's Republic of China.

TenCate, (2015). Mirafi H2Ri woven geosynthetic specifications. Available at: https://www.tencategeo.us/media/39ff27e9-96f5-4450-9aaa-bd9c1cce3160/yV_goA/TenCate%20Geosynthetics/Documents%20AMER/Product%20Description%20Sheets/Woven%20Product%20Description%20Sheets/PDS_H2Ri0417.pdf (Accessed April 26, 2018).

Wang, F., Han, J., Zhang, X., and Guo, J. (2017). Laboratory tests to evaluate effectiveness of wicking geotextile in soil moisture reduction. *Geotext. Geomembranes* 45 (1), 8–13. doi:10.1016/j.geotexmem.2016.08.002

Zaman, M. W., Han, J., and Zhang, X. (2022). Evaluating wettability of geotextiles with contact angles. *Geotextile Geomembranes* 50, 825–833. doi:10.1016/j.geotexmem.2022.03.014

Zhang, C., Miao, C., Zhang, W., and Chen, X. (2018). Spatiotemporal patterns of urban sprawl and its relationship with economic development in China during 1990–2010. *Habitat Int.* 79, 51–60. doi:10.1016/j.habitatint.2018.07.003